WPPFC-CPR(18) 18756

J Karhunen et al.

SOLPS 5.0 modelling of inner divertor detachment in L mode at ASDEX Upgrade with non-diffusive radial SOL transport

Preprint of Paper to be submitted for publication in Proceeding of 23rd International Conference on Plasma Surface Interactions in Controlled Fusion Devices (PSI-23)

This work has been carried out within the framework of the EUROfusion Consortium and has received funding from the Euratom research and training programme 2014-2018 under grant agreement No 633053. The views and opinions expressed herein do not necessarily reflect those of the European Commission.

SOLPS 5.0 simulations of the high-field side divertor detachment of L-mode plasmas in ASDEX Upgrade with convection-dominated radial SOL transport

J. Karhunen[a*], M. Groth[a], D.P. Coster[b], D. Carralero[b,c], L. Guimarais[d], V. Nikolaeva[d], S. Potzel[b], T. Pütterich[b], F. Reimold[e], A. Scarabosio[b], E. Viezzer[b,f], M. Wischmeier[b] and the ASDEX Upgrade Team

[a]*Aalto University, Department of Applied Physics, Espoo, Finland*
[b]*Max-Planck-Institut für Plasmaphysik, Garching, Germany*
[c]*Asociación EURATOM-CIEMAT para Fusión, Madrid, Spain*
[d]*Instituto de Plasmas e Fusão Nuclear, Instituto Superior Técnico, Lisboa, Portugal*
[e]*Max-Planck-Institut für Plasmaphysik, Greifswald, Germany*
[f]*Department of Atomic, Molecular and Nuclear Physics, University of Seville, Seville, Spain*

[*]Corresponding author email: juuso.karhunen@aalto.fi

Abstract

SOLPS 5.0 simulations assuming convection-dominated radial ion transport show qualitative and quantitative agreement with measurements of detached high-field side (HFS) divertor conditions for unseeded low-power L-mode plasmas in ASDEX Upgrade, while simultaneously maintaining a reasonable match to the density and temperature measurements at the low-field side (LFS) and HFS midplanes within the scatter of the data. The decreased diffusive transport from the high-density region in the HFS divertor volume across the separatrix into the core enables spatial extension of the high-density front to above the X-point in agreement with spectroscopic measurements. The suppressed ion fuelling from this region into the core plasma allows increasing the neutral D_2 fuelling to experimental levels, leading to agreement with the measured sub-divertor neutral fluxes within 30%. Detachment of the HFS divertor is observed as a significant decrease of the target ion flux and as reproduction of the characteristic roll-over behaviour of the integrated target ion current at increasing upstream density.

1. Introduction

Operation in detached divertor conditions will be essential to avoid excessive damage of the divertor targets under the heat loads of ITER and future fusion reactors. However, despite the importance of the issue, development of a coherent methodology for achieving agreement between experiments and SOLPS 5.0 [1] simulations for both upstream and detached divertor conditions has proved challenging in existing tokamaks, such as ASDEX Upgrade [2—5]. This has been the case especially in the high-field side (HFS) divertor, where the simulations tend to underestimate the degree of detachment in comparison to measurements.

In earlier SOLPS studies of divertor detachment in ASDEX Upgrade, adjusting the radial transport model for enhanced perpendicular ion transport in the SOL has, in combination to activation of cross-field drifts, been one of the key methods in bringing the solutions closer to the measured divertor conditions. Assuming a purely diffusive model in [4], an overestimation by a factor of 3—4 remained between the simulated and measured HFS target ion flux in L mode. Reduction to experimental levels was achieved in L mode in [5] by

postulating a significant increase of the radial diffusion coefficient to $D_\perp$ ~100—10000 m^2s^{-1} below the X-point in the divertor SOL. More recently in [6], a global decrease of $D_\perp$ close to the separatrix with an addition of a convective velocity term outwards in the low-field side (LFS) SOL was found to successfully yield the experimentally observed formation of the HFS high-density front [7] and detachment of the HFS divertor in H mode.

In this contribution, a convection-dominated radial transport model was applied in SOLPS 5.0 to mimic non-diffusive transport phenomena in L-mode simulations. The transition from the diffusive-convective model applied in [6] towards primarily non-diffusive SOL transport concurs with the current understanding of the radial SOL transport exceeding the neoclassical predictions of diffusion by 1—2 orders of magnitude [8—10] with enhanced far-SOL transport carried by convective filaments [11—13]. The revised transport model was, by default, expected to prevent excessive diffusive leakage of the HFS high-density front from the HFS divertor across the separatrix into the core, which was found essential to allow increasing the neutral fuelling rates to experimental levels in [6].

2. Simulation set-up

The prospects of the convection-dominated radial transport model in SOLPS 5.0 were investigated by simulating the plasma conditions during a deuterium-only, low-power L-mode density scan in ASDEX Upgrade (discharges #32130—33 and #32136 [14]). In these discharges, the HFS divertor conditions ranged from high-recycling (#32130—32) to detached (#32133, #32136) regimes. This work concentrates on the HFS divertor conditions in the detached cases #32133 and #32136, while simulations in the high-recycling conditions are presented only to illustrate the development of the studied quantities over a wider upstream density range and, together with the LFS divertor conditions, will be reported in more detail elsewhere.

A simulation grid was generated according to the magnetic geometry of discharge #32132 at 4.0 s and appended with the sub-divertor structure applied in [6, 15], providing an improved neutral conduction model and an experimentally relevant implementation of the cryopump and the turbomolecular pump. The plasma was fuelled through the divertor dome with a constant D_2 fuelling rate of 1.2—1.4×10^{22} s^{-1}, corresponding to the fuelling rates of the studied discharges. An exception is the highest-density case, #32136, for which the fuelling rate could not be increased above 80—90% of the experimental value to avoid excessive increase of the simulated plasma density in the pedestal and separatrix region. The remaining mismatch may indicate inadequate optimization of the radial transport coefficients but might also partially be due to residual wall pumping, which is not taken into account in the simulations. Constant input power of 0.55 MW was applied through the core boundary with an equal division between electrons and ions. The input power was estimated by subtracting the measured main chamber radiation from the total heating power of each discharge and adjusted to provide the best correspondence to the experiments. The imposed D_2 fuelling rates and input powers are presented in table 1 together with the resulting separatrix electron densities at the LFS midplane.

The radial ion transport was modified from the traditional anomalous diffusion model by decreasing the ion diffusivity in the SOL by an order of magnitude to $D_\perp \sim 0.01—0.1\ m^2s^{-1}$, as shown in figure 1a. The anomalous convective velocities in figure 1b were applied to provide radial ion transport outwards in the SOL, compensating for the decreased diffusive flux to avoid excessive steepening of the radial density profiles. As shown in figures 1d and f for discharge #32136, this results in the applied anomalous convection dominating the radial SOL transport both in the main chamber and in the HFS divertor. Qualitatively similar observations are made for discharge #32133. The radial currents in figures 1d—g were obtained by integrating the radial profiles of the total radial ion flux, as well as its components due to diffusion, applied anomalous convection and drifts, poloidally in the main chamber and below the X-point, respectively. Due to the lack of measurement data of the ion temperature in the SOL, identical radial heat conduction coefficients in figure 1c were used for electrons and ions. To account for the ballooning nature of the radial transport, a B^{-1}-dependent scaling was applied on all of the transport coefficients, resulting in a decrease by approximately a factor of 2 in their values between the LFS and HFS midplanes.

The described radial ion transport model deviates from that used in [6] by having low $D_\perp$ radially across the SOL and the convective radial velocities applied poloidally everywhere instead of only in the separatrix region and the LFS SOL, respectively. Consequently, the radial ion transport is dominated by convection throughout the SOL, as presented in figures 1d and f. In initial tests, the convection-dominated model showed better correspondence to the measured HFS SOL conditions than a model similar to that in [6]. However, it is noted that the approach of [6] was not thoroughly tested in this work due to timing restrictions, and the convection-dominated model is considered as an alternative to – rather than replacement of – the model used in [6].

Cross-field drifts were found essential in advancing the correspondence between the simulations and the experiments in [4, 6], especially in terms of replicating the experimentally observed asymmetries between the HFS and LFS divertors. Therefore, the drift terms were activated in all simulations presented in this work. This required decreasing the time step of the simulations to the order of 10^{-6} s. As a consequence, full convergence of the highest-density case was not achieved within the timeframe of the studies, but variations within 10% are still observed in the total number of particles and the upstream separatrix density during a run. Hence, the solutions may not represent the final state of the given simulation configuration but can still be seen indicative in terms of the prospects of the applied radial transport model.

For reference, results from a generic SOLPS 5.0 density and power scan from [16], with a purely diffusive radial transport model and drift terms activated, are also presented. As shown in figure 1a, the radial diffusivity was approximately an order of magnitude higher in these simulations than with the convection-dominated radial transport model. Figure 1e also indicates that the diffusive radial transport is significantly weaker than the convective transport at corresponding upstream density in figure 1d. In the HFS divertor below the X-point, radial transport is dominated by drift-driven convection, consisting primarily of the E×B drift. The scans, utilizing a feedback fuelling scheme for setting the LFS midplane separatrix density, cover the upstream density and input power ranges of the experiment but

did not aim at accurately reproducing the investigated discharges through optimization of the radial transport parameters. Therefore, they provide primarily a qualitative comparison of the behaviour of the different studied quantities between the two transport models.

3. Simulated plasma conditions

3.1 Upstream n_e and T_e profiles

The LFS density profiles in figures 2a and b are reasonably matched in the simulations within the scatter of the experimental data from measurements by core and edge Thomson scattering, Li beam and the reciprocating probe in the far SOL. An exception is the pedestal density of discharge #32133, which was underestimated by approximately 25%. Moreover, the simulated density profile of discharge #32136 follows the high end of the experimental data, suggesting an apparent overestimation, which may have a significant effect on the simulated divertor conditions due to their strong dependence on the upstream density. On the HFS, the simulated density profiles fit within the data from reflectometry measurements. The simulations also replicate the spreading of the HFS high-density front up to the midplane in discharge #32136.

The simulated electron temperature profiles at the LFS midplane in figures 2c and d follow systematically the low end of the data from measurements by core and edge Thomson scattering, ECE radiometry and the reciprocating probe. This suggests inadequate optimization of the radial heat conduction coefficients or incorrect assumption of the position of the separatrix, whose actual position is more likely to be 0.5—1.0 cm closer to the outer wall [17]. This uncertainty is indicated by the grey regions in figure 2, but the issue could not be properly considered within the timeframe of the studies. In addition to decreasing the upstream separatrix temperature, shifting the separatrix position outwards would decrease the upstream separatrix density by approximately 15—30%. Matching such changes in the upstream conditions in the simulations can be expected to have significant effects on the target conditions, and, consequently, the consistency between these simulations and the investigated discharges needs to be further addressed in future studies. Hence, the comparison between the presented simulations and the experiment is used merely as a guideline for studying the behaviour of the plasma conditions with respect to experimental observations. Rather than accurate reproductions of the investigated discharges, the results are considered as an indicative demonstration of the prospects of the non-diffusive approach in improving the description of the HFS divertor detachment in SOLPS 5.0.

3.2 High-density front in the HFS divertor

Consistent description of the HFS high-density front with respect to experimental measurements was found essential in modelling divertor detachment by SOLPS 5.0 in [6]. To compare the simulations to the experimental observations of the formation of the high-density front, given by Stark broadening of the D_δ emission line, the spectroscopic measurements were synthesized in the post-processing of the simulations. This was done by using the code output for the electron temperature, electron density and neutral D density to evaluate the Stark-broadened D_δ line profiles with the help of ADAS data [18] and methods presented in

[19]. The synthetic measurement was performed by integrating the line profiles along the spectroscopic lines-of-sight presented in figure 3, whose geometry is identical to the ones used in the experimental measurements. The synthetic measures for the divertor density were given by the widths of the synthetic emission lines, integrated along the lines-of-sight.

The experimental data in figure 4 show approximately 2—6 times higher densities in the HFS divertor volume than in the core plasma in the studied discharges. The horizontal RXV lines-of-sight indicate an increase in the divertor density by a factor of 2—3 vertically upwards from the strike-point region towards the X-point in both discharges. In discharge #32133, the density appears to peak approximately at the vertical level of the X-point, observed by the RXV5 line-of-sight. The decrease towards the RXV6 line-of-sight is followed by only scarce density data from the RXV7 line-of-sight, indicating a steep decrease in the divertor density to levels predominantly below the detection limit of the Stark broadening measurements. In discharge #32136, the increase in the density continues above the X-point, suggesting wider poloidal extension of the high-density front. This is also supported by the reflectometry measurements of the radial density profile at the HFS midplane showing significantly higher values than on the LFS in figure 2b, which was not as clearly observed for discharge #32133. The vertical ZIV lines-of-sight do not show clear variations in the measured divertor densities in the horizontal direction in either of the discharges. In discharge #32136, the ZIV7—9 lines-of-sight suggest an increase in the density by up to a factor of 2 in the vicinity of the X-point in comparison to the proximity of the HFS target, but the interpretation is challenged by the simultaneous increase in the scatter of the spectroscopic data. The described behaviour of the HFS divertor density is consistent with earlier spectroscopic observations in L-mode density scans [7].

The simulations with the convection-dominated radial transport model reproduce the measured profiles of the density profiles qualitatively and mostly also quantitatively within the statistical variation of the spectroscopic data. For discharge #32133, the simulations show stronger decrease in the density above the X-point than the measurements with an underestimation of up to 50% with respect to the RXV5—6 lines-of-sight. In the horizontal direction, the simulations of discharge #32133 also overestimate the density close to the HFS target, given by the ZIV1—3 lines-of-sight, by up to a factor of 2—3. For discharge #32136, quantitative agreement with the measurements is achieved within the scatter of the data in both directions with the density showing increase towards the X-point both vertically and horizontally.

In contrast, the density and power scans with the fully diffusive radial transport model show qualitatively opposite behaviour of the divertor density in comparison to both the experimental data and the convection-dominated simulations. In both density cases, the density is the highest close to the strike point and decreases significantly towards the X-point in both vertical and horizontal directions. This points at strong peaking of the density in the near SOL close to the target, which is characteristic to the high-recycling conditions in which the HFS divertor remained in the fully diffusive simulations, as discussed in section 3.3. The observed qualitative behaviour of the density is fairly consistent with the results in [4], in which the fully diffusive radial transport model also could not reproduce the increase of the divertor density towards the X-point, especially in the horizontal direction. As observed earlier in experiments [20] and SOLPS simulations [6], the divertor density increases with

input power, which explains the range of variation of the results at each upstream density for which results with P_{in} = 0.5—0.6 MW are presented, visualized by the shaded green region in figure 4.

As indicated by the significant qualitative differences in the spatial distributions of the divertor density between the two radial transport models, decreasing the diffusive transport from the divertor volume across the separatrix into the core provides means for predicting the evolution of the divertor density close to the X-point in agreement with experimental measurements. This is supported by figure 5a, which presents the radial ion fluxes across the separatrix immediately above the X-point in the HFS SOL, normalized to the LFS midplane separatrix density to eliminate the direct effect of increased density on the flux for better representation of the strength of the transport. For wider presentation of the evolution of the transport, also results for the simulations in high-recycling conditions are presented. With the fully diffusive model, radial transport is increased towards the core, as the HFS high-density front is formed at high upstream densities, preventing its evolution in the X-point region in consistence with experimental observations. Instead, the convection-dominated simulations show transport away from the core at all densities, albeit with a reduction in the case of discharge #32133. This indicates that the suppressed inward-directed diffusive component, whose magnitude is only approximately 2% of the total flux, is completely overcome by convection outwards: approximately 85% of the total flux is due to the applied anomalous convection with the remaining part covered primarily by the $\nabla B \times B$ drift. This is in contrast to [6], where some diffusive inward transport remained above the HFS X-point, contributing to the fuelling of the core plasma.

At the LFS midplane, similar investigation indicates enhanced radial transport with increasing upstream density in the convection-dominated simulations. Since radial transport due to the $\nabla B \times B$ drift is insignificant in comparison to the applied convective transport at the midplane, where the flux surfaces are almost vertical, this reflects directly the applied velocities in this region in figure 1. The need for increasing the convective velocities to match the increasing upstream densities is qualitatively consistent with experimental observations of enhanced radial filamentary transport at high densities in L-mode plasmas in ASDEX Upgrade [21—23]. In contrast, the fully diffusive model with identical diffusion coefficients throughout the density scan shows weakening of the transport with increasing upstream density.

As discussed in [6], the improvement in retaining the high-density front in the divertor volume assists in allowing the increase of the neutral fuelling rates in the simulations to the experimental levels due to the decreased ion fuelling of the core plasma by diffusive transport from the HFS divertor. This is supported by comparison to the fully diffusive simulations: without the refined radial transport and the suppressed ion fuelling from the HFS divertor, the D_2 fuelling rates set by the density feedback to reach similar upstream densities are 2—3 times lower than with the convection-dominated transport model.

3.3 HFS target conditions

The radial profiles of the HFS target ion flux in figures 6a and b were reasonably matched between the convection-dominated simulations and the Langmuir probe data, indicating

partial and full detachment of the vertical part of the HFS target within $\Delta S < 10$ cm for discharge #32133 and #32136, respectively. Here, the coordinate ΔS measures the distance from the HFS strike point along the target plate such that positive ΔS is in the SOL. The correspondence between the simulations and the experiments is, consequently, improved from the purely diffusive simulations in [4], in which the HFS target ion flux was overestimated by a factor of 3—4 at high upstream densities. In the case of discharge #32133, the detached region is, however, narrower than in the experiment. The characteristics of detachment are seen also as reproduction of the roll-over of the HFS target ion current, obtained by integrating the target ion flux over the area of the target plate, at high densities within the scatter of the Langmuir probe data in figure 7a. For better presentation of the evolution of the divertor conditions, also the simulations and experimental data of the high-recycling conditions, as well as probe data from the density-ramp discharge #32125 of the same experiment, are presented in figure 7. In contrast to the convection-dominated model, the peak value of the target ion flux in figures 6a and b decreased by approximately only 10% in the density and power scans with the fully diffusive radial transport model, as the upstream density is increased within the range of the presented discharges. The HFS target thus remained in high-recycling conditions, which is also seen in figure 6a as saturation rather than roll-over of the integrated target ion current.

Both transport models show a decrease in the strike-point electron temperature from 5—20 eV to below 1 eV with increasing upstream density in figure 7b with the convection-dominated transport model yielding a reasonable agreement within the scatter of the probe data. However, at the highest densities, the comparison between the simulations and the experimental data is challenging due to the significant uncertainty of temperature measurements by Langmuir probes at low temperatures, especially below 3 eV [24]. This is the case particularly in the detached regions within $\Delta S < 10$ cm in figures 6c and d, where the simulations show target electron temperatures at or below 1 eV for both discharges #32133 and #32136, while the measured temperatures are in the range of 1—4 eV. In the far SOL, the simulations still appear to underestimate the target temperature by a factor of 4—6. This is likely a consequence of remaining inconsistencies in power balance in the simulations. With the fully diffusive radial transport model, the target temperatures are within 0.5—2 eV similar to the convection-dominated model.

3.4 Sub-divertor neutral fluxes

The closest comparison of the neutral conditions in the HFS divertor between the experiment and the simulations is provided by the sub-divertor ionization pressure gauge measurements of the neutral fluxes. These measurements were synthesized in the simulations by transparent EIRENE test surfaces [6], which registered the passing fluxes of neutral atoms and molecules in the locations of the actual pressure gauges. In this work, the analysis concentrates on gauges 1, 4 and 7 below the divertor dome and 19 and 20 behind the HFS target, as shown in figure 8.

Below the divertor dome, the simulations with the convection-dominated radial transport model follow the low end of the data range set by the three pressure gauges, as shown in figure 9a. At the highest density case #32136, however, the simulations still underestimate the neutral fluxes by 15—30% in comparison to the measurements. The underestimation

could partially be attributed to the shortfall of 10—20% in the D_2 fuelling with respect to the experimental value, as discussed in section 2. With the diffusive-only radial transport model, the fluxes observed below the divertor dome are approximately 2—3 times lower than with the convection-dominated model at upstream densities corresponding to discharges #32133 and #32136. This correlates with the D_2 fuelling rates for which the comparison between the two transport models at the highest densities yields the same ratio. Behind the HFS target, both transport models agree with the measurements within the scatter of the experimental data in figure 9b. Of the investigated gauges, the ones below the divertor dome are, however, believed to give a more representative description of the neutral conditions near the HFS divertor target due to the more direct connection between the divertor and sub-divertor regions through the opening between the inner leg and the dome.

4. Conclusions

SOLPS 5.0 simulations with a convection-dominated radial ion transport model were performed with the aim of replicating the detached HFS divertor conditions observed experimentally in unseeded, low-power L-mode discharges in ASDEX Upgrade. For qualitative inspection of the behaviour of the plasma conditions between the different transport mechanisms, a comparison was made to a generic density and power scan with a fully diffusive radial transport model.

The comparison between the simulations and the experiment indicates that the convection-dominated radial transport model yields an improved correspondence of HFS divertor detachment to experiments in L mode with respect to earlier work in, e.g., [2—5], without the need for significant variation of the transport assumptions between the main chamber SOL and the divertor region, as made in, e.g., [5]. Instead, conditions beyond high-recycling could not be achieved with a purely diffusive model. This is attributed to the improvement in retaining the HFS high-density front in the HFS divertor SOL, resulting in its spatial extent to above the X-point in consistence with the experiments. This allows increasing the neutral D_2 fuelling rates to the experimental levels, leading to increased neutral densities in the HFS divertor. With the diffusive-only radial transport model, similar increase of the HFS divertor volume density in the X-point region is balanced by increased diffusive transport from the high-density region across the separatrix into the core. Due to this ion fuelling of the core plasma, significantly lower D_2 fuelling rates could be applied to achieve similar upstream densities as with the convection-dominated model.

According to initial tests, the convection-dominated model was found more suitable for low-power L-mode simulations than a model similar to that in [6] with decreased near-SOL diffusivity and radial convection applied in LFS SOL only. This could potentially be attributed to increased penetration of recycled neutrals into the core due to the factor-of-10 decrease in the input power between the H-mode simulations in [6] and the L-mode simulations in this work: retaining the HFS high-density region in the HFS divertor SOL in the X-point region and avoiding excessive increase of the upstream separatrix and pedestal density with increasing neutral fuelling were found to become increasingly challenging at low input powers without extending the convective transport into the HFS SOL.

The described observations suggest that replacing fully diffusive radial ion transport by a convection-dominated model is a viable approach at modelling detachment of the HFS divertor in ASDEX Upgrade. However, it is emphasized that convection is used merely as an anomalous proxy for non-diffusive transport mechanisms, while the defining quantity in the simulations is the total perpendicular ion flux as a linear combination of the user-defined diffusive and convective components. In this context, the benefit of the convection-dominated model is its ability of providing a total flux without excessive inward transport from the HFS high-density front into the core. With a purely diffusive transport model, this would likely require additional regional transport assumptions near the HFS X-point on top of the applied ballooning scaling.

Since fluid codes in general do not solve the radial ion transport, but the constitution of the radial ion flux relies on the *ad hoc* assumptions of the user with convection normally as the only available alternative to diffusion, claims of the actual phenomena driving the non-diffusive radial ion transport are beyond the scope of this work. Nevertheless, the observations decrease the disagreement between neoclassical predictions of diffusive SOL transport and the typical assumptions of significantly stronger anomalous diffusion in fluid codes, as well as support experimental observations of enhanced convective radial SOL transport in ASDEX Upgrade L-mode plasmas. It is also shown that, in addition to the values of the radial transport coefficients, considering also the nature of the radial transport itself provides an additional tool for matching experimental plasma conditions. Eventually, this points at need for more advanced coupling of fluid codes to first-principle modelling of the radial transport and better understanding of the transport phenomena.

References

[1] R. Schneider et al., Contributions to Plasma Physics **46** (2006) 3–191
[2] M. Wischmeier et al., Journal of Nuclear Materials **390—391** (2009) 250—254
[3] M. Wischmeier et al., Journal of Nuclear Materials **415** (2011) S523—S529
[4] L. Aho-Mantila et al., Plasma Physics and Controlled Fusion **59** (2017) 035003
[5] M. Wischmeier et al., 24th IAEA Fusion Energy Conference (2012) EX/P5-34
[6] F. Reimold et al., Nuclear Materials and Energy **12** (2017) 193—199
[7] S. Potzel et al., Nuclear Fusion **54** (2014) 013001
[8] E.J. Doyle et al., Nuclear Fusion **47** (2007) S18–S127
[9] R.J. Groebner et al., Nuclear Fusion **26** (1986) 543–554
[10] W. Fundamenski et al., Nuclear Fusion **47** (2007) 417—433
[11] M.V. Umansky et al., Physics of Plasmas **5** (1998) 3373—3376
[12] S.I. Krasheninnikov, Physics Letters A **283** (2001) 368—370
[13] A. Loarte et al., Nuclear Fusion **47** (2007) S203—S263
[14] J. Karhunen et al., Nuclear Materials and Energy **12** (2017) 935—941
[15] F. Reimold et al., Journal of Nuclear Materials **463** (2015) 128–134
[16] J. Karhunen, PhD Thesis, Aalto University (2018)
[17] E. Wolfrum, private communication (2018)
[18] H.P. Summers, *The ADAS User Manual*, version 2.6 (2004), www.adas.ac.uk
[19] B. Lomanowski et al., Nuclear Fusion **55** (2015) 123028
[20] S. Potzel et al., Journal of Nuclear Materials **463** (2015) 541–545
[21] D. Carralero et al., Nuclear Fusion **54** (2014) 123005

[22] D. Carralero et al., Physical Review Letters **115** (2015) 215002
[23] D. Carralero et al., Nuclear Fusion **57** (2017) 056044
[24] M. Weinlich et al., Contributions to Plasma Physics **36** (1996) 53–60

Acknowledgements
This work has been carried out within the framework of the EUROfusion Consortium and has received funding from the Euratom research and training programme 20145-2018 under grant agreement number 633053 [and from Tekes – the Finnish Funding Agency for Innovation under the FinnFusion Consortium]. The views and opinions expressed herein do not necessarily reflect those of the European Commission.
Work performed under EUROfusion WP PFC.

Tables

Table 1

Discharge #	Γ_{D2} (10^{22} s^{-1})	$n_{e,sep,omp}$ (10^{19} m^{-3})	P_{in} (MW)
32133	1.2	2.5	0.55
32136	1.4	3.1	0.55

Table captions

Table 1: D_2 fuelling rates, resulting separatrix densities at the LFS midplane and input powers through the core boundary in the simulations with the convection-dominated radial ion transport model, consistent with ASDEX Upgrade discharges #32133 and #32136.

Figures

Figure 1

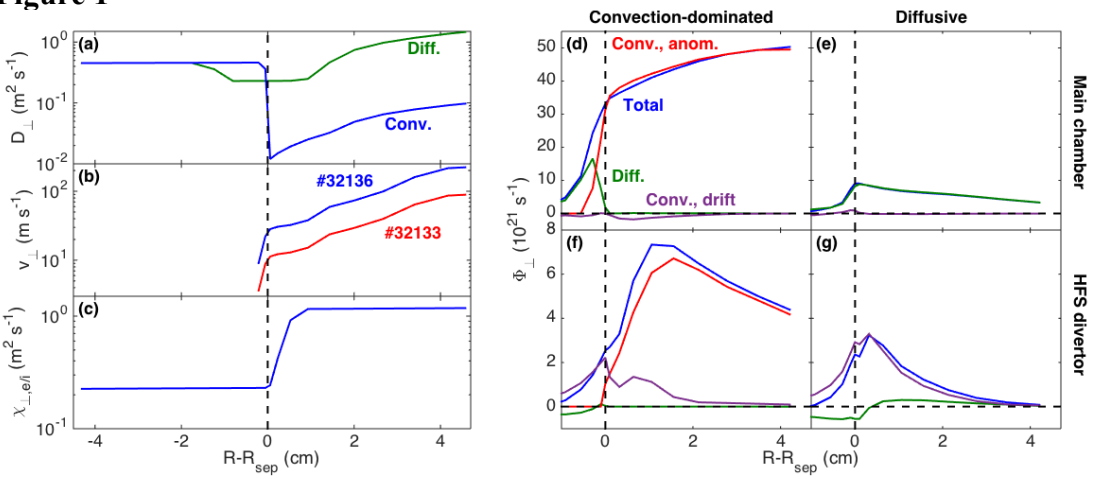

Figure 2

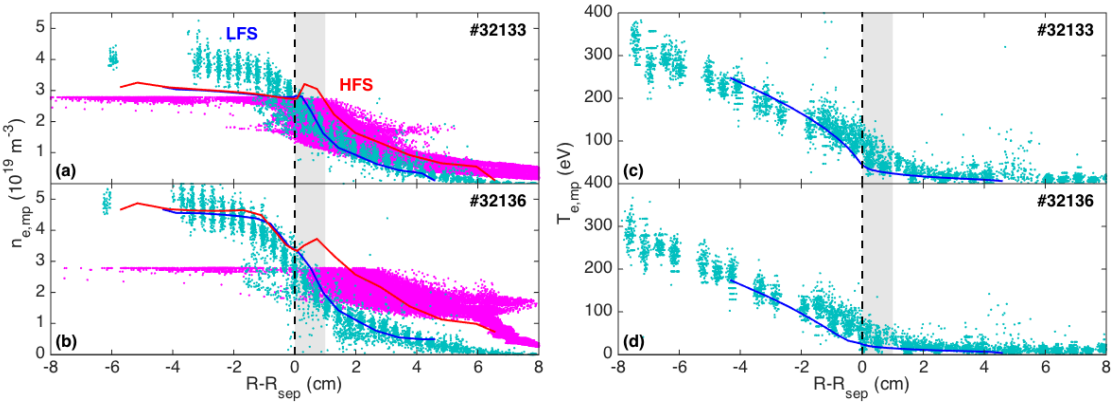

Figure 3

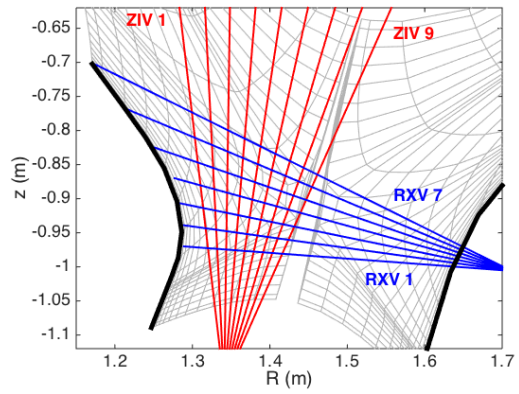

Figure 4

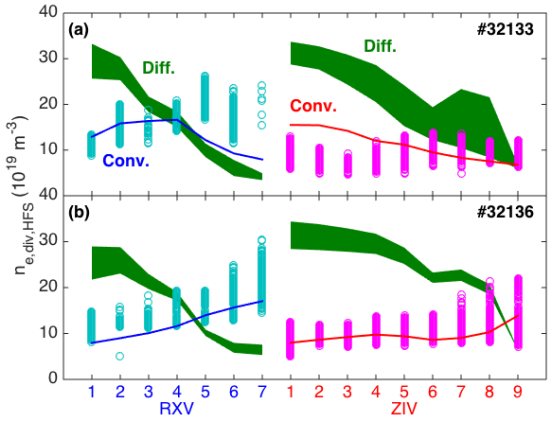

Figure 5

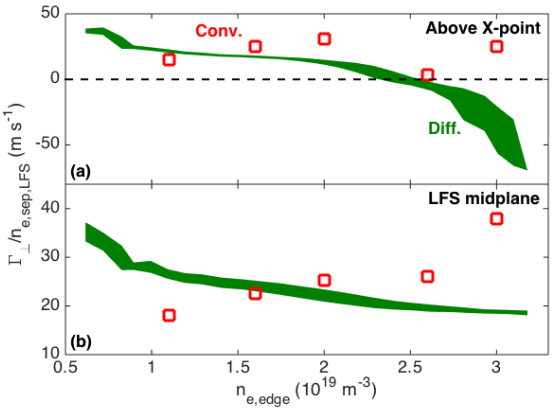

Figure 6

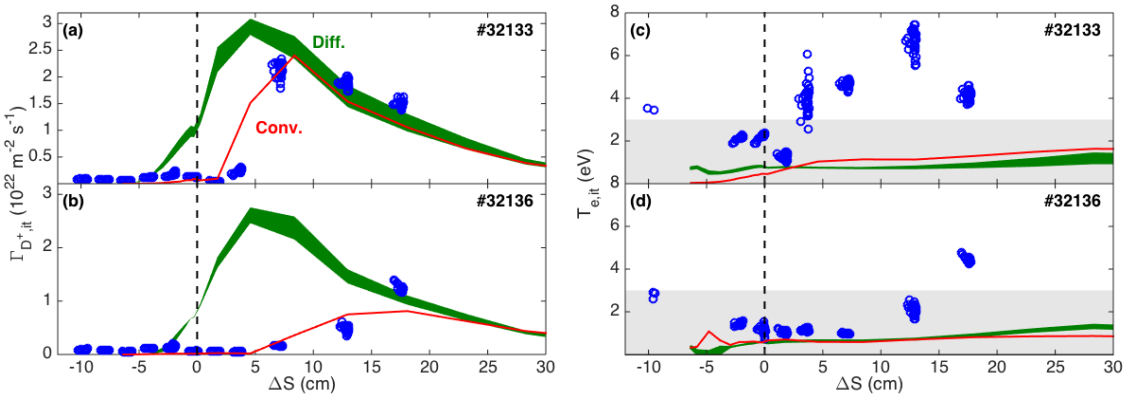

Figure 7

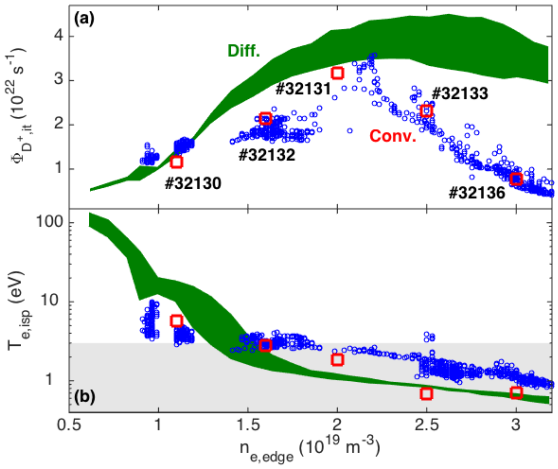

Figure 8

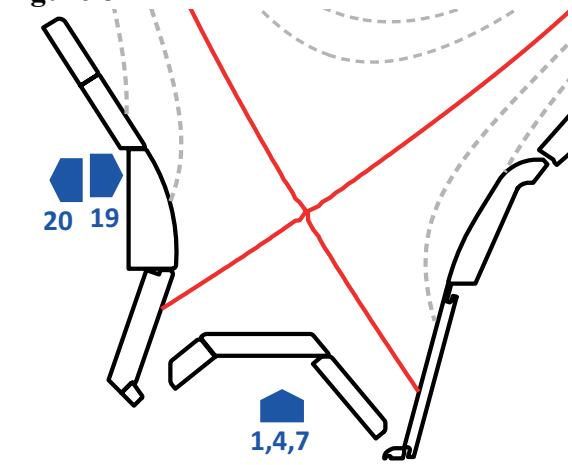

Figure 9

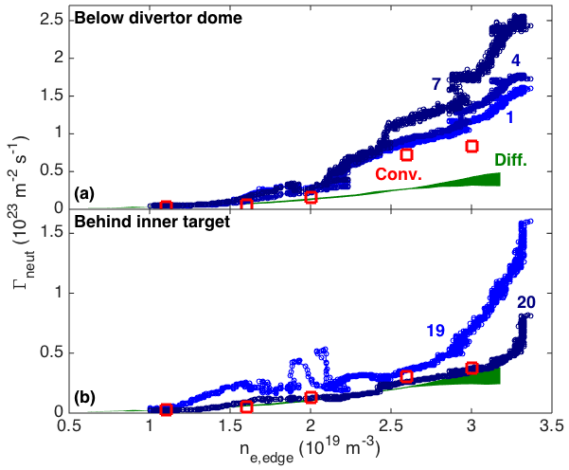

Figure captions

Figure 1: Radial ion diffusion coefficients (a), convective ion velocities (b) and electron and ion heat conduction coefficients (c) applied in the simulations. The profiles are presented at the LFS midplane, while the values are lower by approximately a factor of 2 at the HFS midplane due to the B^{-1} dependence of the ballooning scaling. The green curve in (a) corresponds to the radial diffusivity in the generic density and power scans used for qualitative comparison between the convection-dominated and fully diffusive transport models. The positive direction in (b) is outwards from the separatrix towards the wall. Radial profiles of poloidally integrated radial ion fluxes in the main chamber SOL (d,e) and the HFS divertor SOL (f,g) for the highest-density case #32136 of the convection-dominated simulations (d,f) and the corresponding upstream density of the fully diffusive simulations at an input power of P_{in} = 0.5 MW (e,g). The colour coding for the total flux (blue) and its components due to diffusion (green), applied anomalous convection (red) and drifts (purple) applies for all figures (d—g). The profiles are mapped to the LFS midplane.

Figure 2: Comparison of the radial profiles of electron density (a,b) and electron temperature (c,d) at the LFS (blue) and HFS (red) midplanes between the simulations (solid curves) and the experiment (data points) for discharges #32133 (a,c) and #32136 (b,d). The grey regions indicate the uncertainty of the position of the separatrix.

Figure 3: Spectroscopic lines-of-sight used for measuring the electron density in the HFS divertor volume in the experiment, as well as in post-processing of the simulations. The numbers of the lines-of-sight increase vertically upwards for the RXV lines-of-sight (blue) and from the HFS towards the LFS for the ZIV lines-of-sight (red). The simulation grid is presented in grey in the background, while the thick black curves mark the divertor targets.

Figure 4: Comparison of the electron densities in the HFS divertor volume between post-processed simulations (solid curves) and spectroscopic measurements (data points) for discharges #32133 (a) and #32136 (b). The green shaded regions represent the density and power scans with fully diffusive radial transport at upstream densities corresponding to the studied discharges and input powers of P_{in} = 0.5—0.6 MW. The geometry of the horizontal RXV (blue) and vertical ZIV (red) lines-of-sight is presented in figure 3.

Figure 5: Radial ion fluxes across the separatrix above the HFS X-point (a) and at LFS midplane (b) as functions of the upstream edge density in the convection-dominated (red squares) and fully diffusive (green regions) simulations. The green shaded regions represent the density and power scans with fully diffusive radial transport with input powers of P_{in} = 0.4—0.6 MW. The fluxes have been normalized to the separatrix density at LFS midplane to eliminate the direct effect of the increasing density on the flux. The positive direction is outwards, while negative fluxes are towards the core. For wider presentation of the development of the radial transport, also results for the high-recycling cases #32130—32 are presented.

Figure 6: Comparison of the HFS target ion flux (a,b) and electron temperature (c,d) between simulations (solid curves) and target Langmuir probe measurements (data points) for discharges #32133 (a,c) and #32136 (b,d). The green shaded regions represent the density and power scans with fully diffusive radial transport at upstream densities corresponding to the studied discharges and input powers of P_{in} = 0.5—0.6 MW. The coordinate ΔS measures the distance from the HFS strike point along the target plate such that positive ΔS is in the SOL. The grey regions in (c,d) indicate the region below 3 eV in which the uncertainty of the probe data is significant.

Figure 7: Comparison of the integrated HFS target ion current (a) and the HFS strike-point electron temperature (b) as functions of the upstream edge density between the simulations (red square data points) and target Langmuir probe measurements (blue circular data points). For wider presentation of the development of the detachment of the HFS divertor, also results for the high-recycling cases #32130—32 are presented. The green shaded regions represent the density and power scans with fully diffusive radial transport with input powers of P_{in} =

0.4—0.6 MW. Note the logarithmic scale in (b). The grey region in (b) indicate the region below 3 eV in which the uncertainty of the probe data is significant.

Figure 8: Locations of the ionization pressure gauge measurements of the sub-divertor neutral fluxes in ASDEX Upgrade below the divertor dome and behind the HFS target. In the simulations, the measurements were synthesized by EIRENE test surfaces in the same locations.

Figure 9: Comparison of the sub-divertor neutral flux below the divertor dome (a) and behind the HFS target (b) as a function of the upstream edge density between the simulations (red square data points) and ionization pressure gauge measurements (blue circular data points). To visualize the steep increase in the neutral density in the course of detachment, also the results for the high-recycling cases #32130—32 are presented. The green shaded regions represent the density and power scans with fully diffusive radial transport with input powers of P_{in} = 0.4—0.6 MW. The locations of the labeled pressure gauges are presented in figure 8.